IEEE Access
Multidisciplinary | Rapid Review | Open Access Journal

Received August 25, 2016, accepted October 7, date of publication November 16, 2016, date of current version February 20, 2017.

Digital Object Identifier 10.1109/ACCESS.2016.2629672

The Efficiency of a Two-Stage Reluctance Accelerator Through Pulse Shaping

MICHAEL J. HARRIS, M. SHAIKH, B. T. BRISTOLL, K. VINE, AND PAUL A. BARTLETT
Department of Physics and Astronomy, University College London, London, WC1E 6BT, U.K.
Corresponding author: P. A. Bartlett (paul.bartlett@ucl.ac.uk)

ABSTRACT An investigation considering the efficiency gains of electrical pulse-shaping for a two-stage reluctance accelerator system has been undertaken. An optimum gross efficiency of $(1.36 \pm 0.02)\%$ was achieved, amounting to an increase of $(290 \pm 20)\%$ relative to the performance of an equivalent single-stage accelerator. The performance increase due to pulse-shaping for a two-stage setup was found to surpass that achieved for this single-stage setup in terms of both efficiency and velocity. This investigation highlights the potential of pulse-shaping methods to increase the feasibility and flexibility of electrical acceleration for a variety of practical applications. The intention of this paper was to exhibit the potential of reluctance acceleration technology in multi-stage, initially by using a two-stage system. Possible avenues for further investigation are proposed, to build upon the results of this study.

INDEX TERMS Magnetic circuits, magnetic devices, accelerator magnets, linear accelerators, energy efficiency.

I. INTRODUCTION

Reluctance accelerators are linear motors that can be used to accelerate ferromagnetic projectiles with lower drive currents than other induction machines [1]. In reluctance accelerators, a current pulse is applied to a stator solenoid that generates a transient magnetic field. This field induces an accelerating force on a ferromagnetic projectile that is within the field's influence. It is called a reluctance accelerator as the force acting on the projectile moves it to the location of minimum magnetic reluctance [2]. A reluctance accelerator consists of either a single, or series, of sequentially excited stator solenoids. A single solenoid is configured coaxially with a ferromagnetic projectile so that applying a current pulse to the solenoid accelerates the projectile towards its center due to the induced magnetic field [3]. A series of solenoids can accelerate a projectile from the resultant magnetic forces of sequential current-pulses applied to each solenoid [3]–[5]. In this instance, reluctance can be considered to be the magnetic equivalent to resistance in electrical circuits. The magnetic flux ϕ flowing in a circuit, due to the application of a magnetomotive force (*m.m.f*), is determined by reluctance $\Re$ such that [6]

$$R = \frac{m.m.f}{\phi} = \frac{L}{\mu_0 \mu_r A} \tag{1}$$

where μ_0 is the permeability of free space, μ_r is the relative permeability of the material within the magnetic field, L is the length of the flux-path and A is the cross-sectional area of the solenoid core. The magnetomotive force (*m.m.f*) for such a system can be approximated by (2) [6]

$$m.m.f = NI \tag{2}$$

where N is the number of turns for the solenoid and I is the current flowing through it.

Eq. 2 is analogous to Ohm's law, and suggests that the reluctance and *m.m.f* can be approximated to be equivalent to electrical resistance and potential respectively. This indicates that the *m.m.f* is the total potential that drives magnetic flux around this magnetic circuit. In addition, the magnetic circuit acts to determine the path of minimum reluctance for the magnetic flux to follow.

II. RELUCTANCE ACCELERATOR DESIGN

A typical reluctance accelerator contains the following components: a capacitor bank, a capacitor charging circuit, a stator solenoid (sometimes called the 'drive coil'), a projectile and a triggering circuit. To achieve high projectile accelerations, a current is needed to flow through the coils to generate magnetic fields to attract and accelerate ferromagnetic projectiles. Capacitors are the ideal energy supply option as they store large amounts of charge. This energy is discharged into stator coils providing short-lived current pulses to create the accelerating magnetic force on the ferromagnetic projectile.

A reluctance accelerator is comprised of one or more solenoid coils that can supply kinetic energy to a ferromagnetic projectile. A typical stator solenoid is shown in Fig. 1 [6].

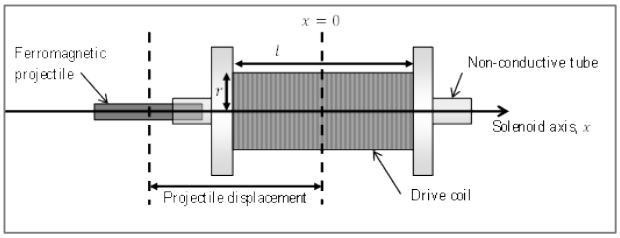

FIGURE 1. Schematic diagram of single solenoid reluctance accelerator displaying the main system components. It shows the position and direction of motion of a ferromagnetic projectile, prior to application of an accelerating pulse, at a distance from the solenoid center (at $x = 0$) [6].

This projectile can be initially at rest or it can have a velocity that has been supplied via the action of a previous stator solenoid. As a projectile approaches a coil, current is applied to the coil to reach a maximum value once the projectile is at a pre-determined position with respect to the center of the stator solenoid. Traditionally, a switch would be closed just before the center of the projectile reaches the center of the coil, in order to allow current from the capacitor bank to flow and exponentially decay to zero through the stator solenoid, as dictated by the time constant of the discharge circuit [2], [6]. A good design for this simple system should ensure that the supply of current to the stator solenoid ends before the centers of the projectile and the stator solenoid coincide. This is to prevent a 'suck-back' effect, where the projectile is exposed to a retarding force that seeks to return it to the center of the solenoid once it has passed this point. This is undesirable if transfer of kinetic energy to the projectile is to be efficient as according to (3) [6], [7]

$$\eta = \frac{K.E.}{U} = \frac{mu_{exit}^2}{C(V_{before}^2 - V_{after}^2)} \tag{3}$$

where m is the mass of the projectile, u_{exit} is the velocity of the projectile after leaving the acceleration system, C is the capacitance of the capacitor that supplies the current pulse and V_{before} and V_{after} are the potential differences (p.d.) measured across the capacitor before and after discharge.

In this investigation, it has been shown that it is possible to further improve the efficiency of single stator solenoid reluctance accelerators by implementing computer-controlled pulse-shaping techniques. This is an improvement on the purely time constant-determined exponential curve shapes used in previously reported systems [6].

III. MULTIPLE STATOR SOLENOID RELUCTANCE ACCELERATOR DESIGN

To investigate the performance of multi-stage reluctance accelerator systems, a device was constructed as seen in Fig. 2.

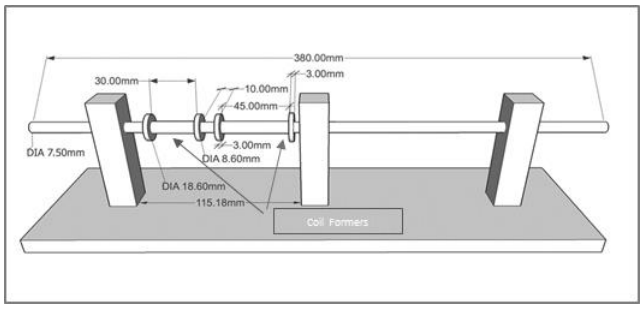

FIGURE 2. Schematic diagram of multi stator solenoid reluctance accelerator. A central glass bore is supported by three Perspex blocks with one 30mm and one 45mm stator solenoid slid onto it (Coil 1 and Coil 2 respectively). The position of these coils could be moved relative to each other.

The configuration of Coil 2, the second-stage, 45mm stator solenoid is shown in Fig. 3.

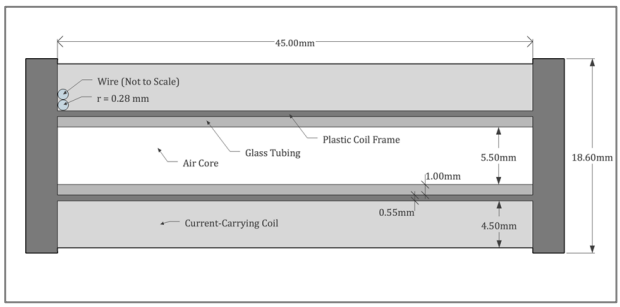

FIGURE 3. Cross-sectional schematic of the 45mm long stator solenoid, showing the dimensions of the constituent components.

The accelerator coils were constructed using a thin polylactic acid (PLA) frame produced from a 3D printer and designed using 3D architectural software. The dimensions are displayed in Fig. 3. The coil lengths were 30mm and 45mm for the Stage 1 and Stage 2 stator solenoids, respectively. The length of Coil 2 was increased in order to account for the non-zero velocity of the projectile at Coil 2, assuming a constant pulse discharge time. A length of 150% of Coil 1 was selected due to its successful application in precedent work [8]. Having partially accounted, in this way, for the difference in projectile velocities, the priority was then to have an equivalent *m.m.f* applied to the projectile at the entry point of each coil. The key benefit was to permit the use of a single set of pulse-shapes for both coils, without requiring a change in the 'driving' circuitry that supplied the current (Fig. 4). Such an equivalent entry *m.m.f* was achieved as follows.

Firstly, the electrical resistance of both coils were set to be the same. The resistance of Coil 2 was made equivalent to that of Coil 1 by equating the length to cross-sectional diameter ratio of the current-carrying wires. Second, assuming constant current, the current-carrying cross-sectional diameter of the stator was set at (18.00±0.02)mm, as shown in Fig. 3. An equation was derived to determine the diameter of wire

required to achieve this assuming a Coil 2 stator length of 45mm (4). That way, a projectile would experience the same magnetic fields when passing through both coils. The derivation was simplified by ignoring the impact of the enamel coating and assuming square packing.

$$d_{w_2}^4 = l_{c_2} \frac{2\alpha_1 r_{w_1}^2}{N_1} \tag{4}$$

In (4), α_1 refers to the number of 'layers' of wire present in Coil 1, $l_{c_2} = (45.0 \pm 0.1)$mm is the length of Coil 2 and r_{w_1} is the radius of the wire used in Coil 1. From previous experiment, $r_{w_1} = (0.50 \pm 0.01)$mm [6]. The wire diameter required for Coil 2 was found to be $d_{w_2} = (0.56 \pm 0.01)$mm. Then, by holding constant the current-carrying diameter and assuming $l_{c_2} = 45$mm it was found that the number of turns for Coil 2, N_2, should ideally equal 648. In practice, Coil 2 was wound to 672 turns due to the requirements of the manufacturing technique. The impact on the resistance from this excess length was not thought to be significant in the context of other sources of uncertainty, in particular the capacitor charging.

As in previous work a ferromagnetic soft iron material, 'Maximag®' was used for the projectile material [6]. Dimensions of the projectile are (25.30±0.01)mm length, (4.08±0.03)mm diameter and a mass of (2.57±0.01)g. This could be placed in the bore tube at the pre-determined distance from coil 1 prior to excitation.

IV. THE RELUCTANCE ACCELERATOR POWER SYSTEM

As in previous work, it was decided that current pulses released from the charged capacitor would incorporate a trigger circuit designed with a solid-state switch to control the discharge [6]. A Fairchild FDL100N50F, 'N-Channel', 500V, 100A MOSFET was used to control the current pulse delivered to the two stator solenoids. The drive circuit for each of the two stator solenoids is shown in Fig. 4.

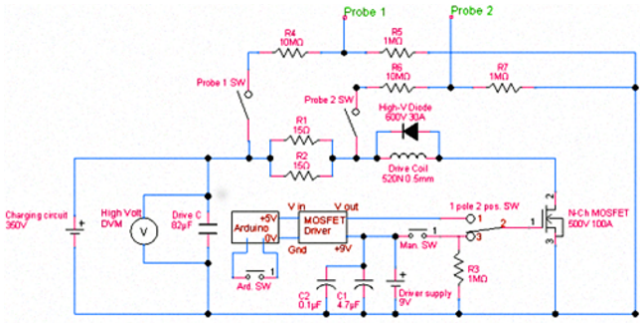

FIGURE 4. Triggering circuit used to control the supply of current from the storage capacitor (shown here as 'Drive C 82μ F') to the drive coil by applying a voltage to the gate of a MOSFET transistor [6].

Fig. 4 shows that two ceramic resistors were used as a way to limit the peak current output to ensure that the components on the circuit board do not operate outside of their design limits. When the capacitor is switched off there is a danger of 'back electromagnetic force (*e.m.f*)' spikes; hence, there is a high-voltage diode, connected across the stator solenoid, as a means of protecting the MOSFET. There is a switch used to manually discharge the capacitor, or a digital discharge using the Arduino-controlled function. Finally, in accordance with proper circuit layout technique, capacitors C1 and C2 are incorporated to bypass the MOSFET driver supply voltage.

The use of a MOSFET allowed for the control of current flow and, therefore, the stator solenoid magnetic field. Essentially, the MOSFET behaves as a variable resistor whose resistance can be controlled via its gate using pulse-width modulated input signals, determined by programming an Arduino Uno microcontroller ('Arduino') with control waveforms [6].

It was possible to allow a 'manual' triggering of the system so that a standard exponential decay-based current could flow through Coil 1 or Coil 2. However, to apply user-defined pulses, the manual trigger circuit in Fig. 4 could be deselected so that an Arduino could control signals to the gate of the MOSFET via a MOSFET driver (Microchip TC4428 1.5A High-Speed Power Driver). This meant that more complex decay currents could be applied to the two solenoids. Both stator solenoids received the same set of pulse shapes from two Arduinos, as discussed. The two microcontrollers could be programmed via USB interface. The capacitor charging circuit used for both stator solenoid systems is as shown in Fig. 5.

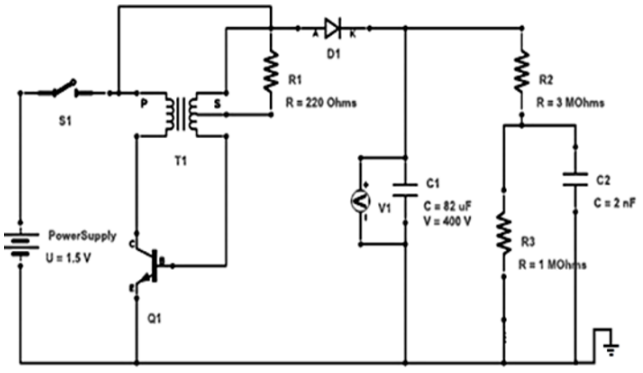

FIGURE 5. Capacitor charging system for each coil. This enabled a 1.5V supply to charge each energy storage capacitor (C1) to 350V.

The overall system can be seen in Fig. 6.

V. THE RELUCTANCE ACCELERATOR SENSOR SYSTEM

Previous work has utilized pick-up coils to measure projectile velocities after acceleration [6]. However, in this work an optical system was devised to overcome some of the low output signal issues with the predecessor coil-based system, using a custom-built photo-interrupter method. Two sensor systems were used, in series, to measure the velocity of the projectile and a second Arduino used to process the output data using an in-built serial monitor.

For each circuit, a phototransistor (Osram Opto SFH 303 FA-3/4 40° (infrared)) (PT) was selected over a

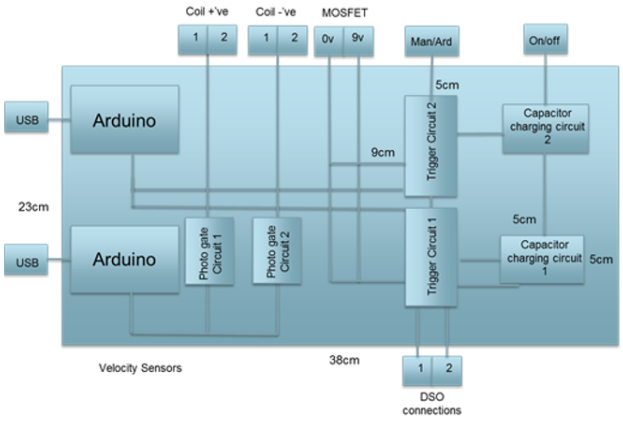

FIGURE 6. Flow chart showing how the two stage reluctance accelerator system was interconnected. The Arduino controllers supply control signals to both MOSFET drivers.

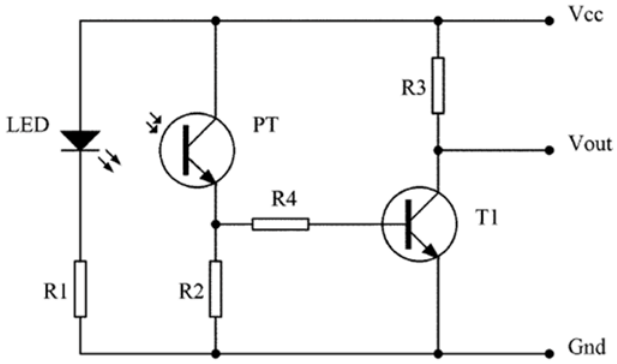

FIGURE 7. Schematic of the photo interrupter system used to measure the velocity of the projectiles moving through the glass bore tube [8].

photodiode because it tends to provide a clearer distinction for on/off logical signals (see Fig. 7) [8]. The light-emitting diode (LED) and PT were selected so as to operate at peak sensitivity in the infrared spectrum, specifically in the range $\lambda = (900 \pm 10)$nm [9]. This allowed the device to function in a well-lit environment. Finally, the logical signal was inverted to be 'low' when activated, by means of incorporating an additional transistor stage and taking the output voltage from its collector. A constant-current voltage $V_{cc} = 5V$ was supplied directly from the Arduino board and V_{out} connected to the Arduino serial monitor input pin (Fig. 7). The light to the phototransistor was supplied by a Vishay TSHF5210 IR LED, 890nm, 20°, with signal amplification by a Fairchild PN2222-ATA bipolar 1A (40V) transistor.

A 3D printed PLA frame, connecting the LED-phototransistor couple to the accelerator apparatus, is shown in cross-section in Fig. 8. This frame was designed with an internal slit of 3mm in diameter to ensure that the LED signal would be blocked entirely by the projectile as it passed down the glass bore tube. The distance between the emitter and receiver was also kept at (24.0±0.1)mm in order to counteract any scattering of light from the cylindrical glass bore.

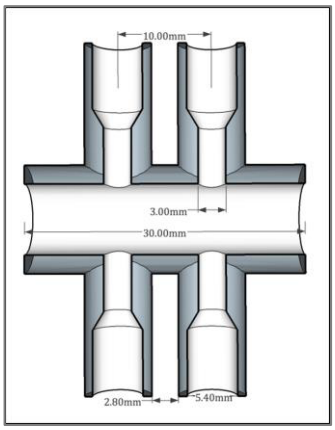

FIGURE 8. Cross-sectional schematic of the photo-interrupter sensor support assembly. LED transmitter and phototransistor receiver pairs face each other with the glass bore tube between them. A projectile passing through the tube interrupts the light signals sequentially, allowing its velocity to be calculated.

Velocity was calculated using the time elapsed in the sensing mechanism to within an uncertainty of ±0.06ms. The on-board clock of the microcontroller is stated as accurate to 4μs by the manufacturer [10]. The higher uncertainty estimate used in practice accounted for: small variations in the logical switch times as the projectile passed the sensor system and in the capacitor initial voltage, and uncertainty in capacitance.

VI. EXPERIMENTAL MEASUREMENTS

As with previous work [6], the optimal starting position for the ferromagnetic projectile undergoing purely exponential decay was obtained. This was of interest both for verification of the apparatus and for optimization of the unaltered multi-stage run that would be performed later.

Optimum starting positions of $x_1 = -(19.50 \pm 0.06)$mm for Coil 1 and $x_2 = -(24.00 \pm 0.06)$mm for Coil 2, relative to the respective coil centers, for a constant initial capacitor charge, were identified. These estimates informed the ideal time-delay range required prior to discharging the second capacitor, given a fixed distance between the two coils. This could be adjusted for different capacitance charges, which is linked to the energy that can be supplied to the projectile.

Selecting an optimal starting position for the projectile can immediately reduce the 'suck-back' effect. As mentioned previously, further increases in efficiency have been shown to be possible through the truncation and 'shaping' of the current pulse in single-stage systems [6]. This investigation sought to test the application of this method to a multi-stage accelerator. In the first instance, equivalent pulse-shape waveforms were applied to both coils of a two-stage accelerator, to enable comparison of efficiency performance between single-stage and dual-stage systems from a common basis.

The discharge pulses were 'shaped' by varying the effective resistance of the discharge driving circuit in real time, using a pre-programmed Arduino in conjunction with the

MOSFET transistor. The Arduino was capable of delivering a direct-current signal output of ≤ 5.0V at 50mA. Due to the 10V required to fully open the MOSFET transistor, a MOSFET driver (Fig. 4) was a necessary component between the MOSFET and the Arduino. The driver would receive a logical signal from the Arduino to control the output voltage to the transistor. However, the relation between the Arduino output and driver output was non-linear. An Arduino output is defined within a discrete range of 266 voltages, called 'duty cycles' (Fig. 9). A duty cycle of '255' represents a 5V output and a duty cycle of '0' represents a 0V output. Thus, to ascertain a relation between the duty cycle inputs and the driver output, a 'power-function' was derived, using a digital storage oscilloscope (DSO) and the probe points shown in Fig. 4 (Eq. 2). Eq. 2 will thus indicate the resistance of the circuit for a selected microcontroller duty cycle. An example of this is shown in Fig. 9 (which can be seen to be non-linear). Note that both coils had equivalent effective-resistance functions, derived separately by equivalent method.

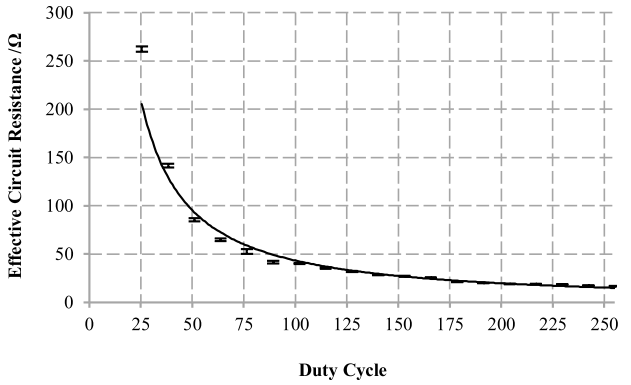

FIGURE 9. The effective resistance of the MOSFET for the Coil 1 circuit. Controlling the pulse width modulation duty cycle applied to the MOSFET gate changes the source/drain effective resistance.

Commands were relayed to the controller using a C++ language variant that has been modified for use with Arduino devices. For optimal precision, the device was set up to run at the highest available clock frequency of 16MHz. This increased the Arduino count rate by 64x and permitted precision to ±0.01ms. However, the change in clock speed increased the command execution rate, which had to be accounted for. It was found that a single interval of the microcontroller 'delay' command at this clock speed, on average, would hold the execution loop for (0.021±0.004)ms Using a 'delay' command enabled a user-defined voltage to be output for a defined period of time, before then allowing the command loop to change the output voltage for the subsequent phase of the pulse shape.

The pulse shapes tested are shown in Fig. 10. Their exact forms were based on those used in previous work [6]. In short, the work in [6] experienced superior efficiency performance from shapes that followed a certain profile; initiate with an above-minimum effective circuit resistance, followed by a period of minimum resistance and a final increase to

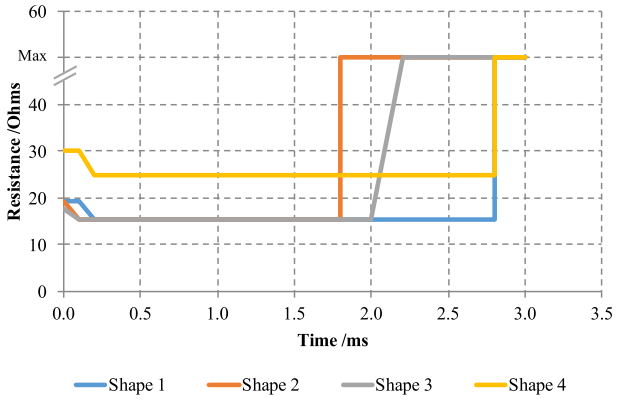

FIGURE 10. Effective resistance profiles applied to the MOSFET gate that modify the shape of the two coils' current flow profiles.

maximum resistance. The time after launch, at which the resistance is increased to maximum, is the dominant factor from an efficiency perspective, since this needs to coincide closely with the time at which the projectile passes the central point of the drive coil. Note in Fig. 10 that the primary differentiator between shapes is their return to maximum resistance. Notice also that the fourth shape is set to a higher 'base' resistance of 25Ω, while still adhering to the waveform of 'Shape 1'. Shape 4 was intended to test the response of the projectile to a more gradual capacitor decay rate, which, with an appropriately-selected truncation time, would accelerate the projectile while retaining a greater capacitor charge post-launch of (100±5)V. Efficiency gains were thereby achievable through both greater retention of energy in the capacitors and the generation of projectile velocity.

After preliminary testing of both coils in single-stage, data was recorded for the two-stage setup over a range of projectile starting positions and with a fixed coil separation of (26.0±0.1)mm. Note that Coil 1 was set to discharge using Shape 1 throughout the experiment, whereas Coil 2 was tested using all four pulse shapes (Fig. 10). The results of these runs are shown in Fig. 11 and Fig. 12.

It was found that Shape 3 was the most efficient shape in second-stage, in contrast to Shape 1 performing best in single-stage runs (Fig. 12). This is thought to be the result of the reduced time to truncation of 2.0ms reducing the 'suck-back' experienced by the projectile in Coil 2. However, the increase in efficiency in all cases is beyond the boundary of experimental uncertainty (Fig. 12). The efficiency increase was the result of contributions from increasing exit velocity and greater residual voltage across the capacitor post-discharge.

Fig. 12 illustrates the immediate increase in efficiency when moving from a single-stage to a multi-stage reluctance accelerator system [11].

Here it has proven possible to quantify the variation; the optimum efficiency increase from an unaltered discharge to a pulse-shaped discharge, in the two-stage setup, was found to be (20±5)% (using Shape 3). This surpassed that observed for single-stage in prior experiment, 0.57%, having used an equivalent set of pulse-shape waveforms [6].

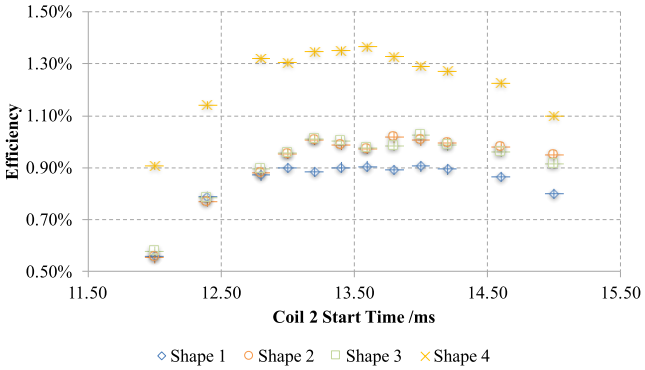

FIGURE 11. Two-stage experimental correlation between recorded efficiency and the time at which Coil 2 is fired after the initial armature launch.

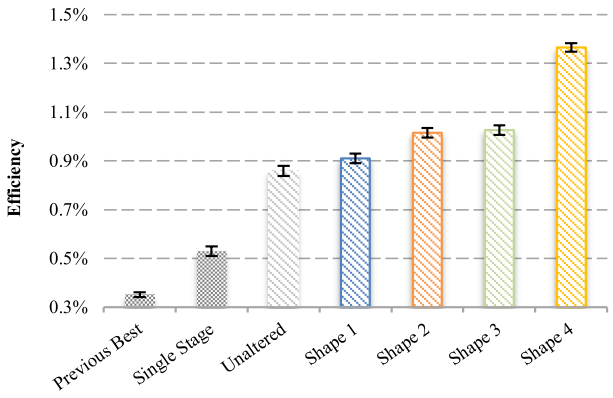

FIGURE 12. Two-stage experimental correlation between the recorded efficiency and the shape format programmed to Coil 2 (Coil 1 is set to 'Shape 1' for all runs). The 'Previous Best' was the highest efficiency reported in [6]. All runs are multi-stage, except for 'Previous Best' and 'Single Stage.'

It would thus appear for these results that the gain in efficiency of pulse-shaping is compounded in the case of multi-stage devices. The underlying cause of this, and the prospect of compounded efficiency gain, would be an apt path of investigation in future work in this field. At this juncture, a case is made for the fundamental benefits of using multi-stage designs and pulse-shaping methods in tandem; not only due to the efficiency gain, but also since they offer fine-tuning options and flexibility that would otherwise be unavailable.

Notice in Fig. 12 the efficiency gain over single-stage recorded from Shape 4, (150±7)%, representing a gross efficiency of (1.36±0.02)%. The reason for the higher efficiency for the lower duty cycle is not yet fully understood and was not anticipated by a preparatory theoretical analysis of the physical system dynamics. A proposed explanation is that the high-frequency modulation (duty cycle), as a digital approximation of an analogue signal, decreases the capacitive reactance, χ_C, of the capacitor, due to intrinsic high-frequency switching as given by (5) [12].

$$\chi_C = \frac{1}{(2\pi fC)} \tag{5}$$

Alternatively, it is plausible that the higher minimum circuit resistance employed in Shape 4 allows the projectile to align more closely with the region of highest force as the discharge rate reaches its maximum, while still truncating at 2.2ms. In other words, the Shape 4 result may imply that there is greater potential for efficiency gain by further reducing the time to truncation below 2.0ms. A pertinent avenue of further investigation, then, would be the construction of pulse shapes of higher resolution, which can be controlled with a precision of ≤0.1ms and within a narrower total timeframe of 2.0ms.

VII. CONCLUSIONS

The investigation demonstrated a (290±20)% efficiency increase, relative to the best single-stage performance in precedent investigation, using Shape 4 [2]. It was observed that the efficiency increase as a result of pulse shaping was proportionately greater when applied to the second stage of a two-stage system, as compared to a single-stage setup (Fig. 12). Future work should consider in greater depth the high performance of Shape 4, i.e. whether the efficiency gains continue to compound, upon introduction of additional stages, and investigate further efficiency-gain potential through higher-resolution pulse shaping.

Progress in developing electrical acceleration mechanisms could lead to the engineering of magnetically accelerated designs with sufficient efficiency to justify industrial application. In many cases, it is this efficiency factor that remains the key hurdle standing between reluctance acceleration technology and such industrial application. More specifically, conceivable uses might include: in-flight spacecraft propulsion and boosting, ground-to-air spacecraft acceleration and aircraft launching, and an environmentally-friendly solution for the next generation of rail transportation. The glimpses into the potential of this technology, from this study and from prior studies, should help to encourage further attention and investment into the field.

REFERENCES

[1] G. W. Slade, "A simple unified physical model for a reluctance accelerator," *IEEE Trans. Magn.*, vol. 41, no. 11, pp. 4270–4276, Nov. 2005.
[2] D. A. Bresie and J. A. Andrews, "Design of a reluctance accelerator," *IEEE Trans. Magn.*, vol. 27, no. 1, pp. 623–627, Jan. 1991.
[3] A. Waindok and G. Mazur, "A mathematical and physical models of the three-stage reluctance accelerator," in *Proc. 2nd Int. Students Conf. Electrodyn. Mechatronics (SCE)*, May 2009, pp. 29–30.
[4] H. Xiang, B. Lei, Z. Li, and K. Zhao, "Design and experiment of reluctance electromagnetic launcher with new-style armature," *IEEE Trans. Plasma Sci.*, vol. 41, no. 5, pp. 1066–1069, May 2013.
[5] L. Zhiyuan, L. Youtian, M. Xueping, X. Hongjun, and C. Shumei, "Dynamic research of multi-stage reluctance coil gun," in *Proc. 17th Int. Symp. Electromagn. Launch Technol. (EML)*, Jul. 2014, pp. 1–4, doi: 10.1109/EML.2014.6920187.
[6] L. M. Cooper, A. R. Van Cleef, B. T. Bristoll, and P. A. Bartlett, "Reluctance accelerator efficiency optimization via pulse shaping," *IEEE Access*, vol. 2, pp. 1143–1148, 2014, doi: 10.1109/ACCESS.2014.2359996.
[7] J. L. Rivas-Camacho, M. Ponce-Silva, and V. H. Olivares-Peregrino, "Experimental results concerning to the effects of the initial position of the projectile on the conversion efficiency of a reluctance accelerator," in *Proc. 13th Int. Conf. Power Electron. (CIEP)*, Jun. 2016, pp. 92–97, doi: 10.1109/CIEP.2016.7530737.
[8] "Design fundamentals for phototransistor circuits," Appl. Note AN-3005, ON Semiconductor, Aurora, Colorado, 2002

[9] RS Components Ltd. *Silicon NPN Phototransistor, Version 1.1, SFH 303 FA Data Sheet, Osram Opto Semiconductors GmbH*. Regensburg, Germany, 2014. [Online]. Available: http://docseurope.electrocomponents.com/webdocs/08b2/0900766b808b2f2c.pdf
[10] Arduino LLC. *Reference: Micros, Arduino Open Resources. Online Resource*, accessed on Mar. 17, 2015. [Online]. Available: http://arduino.cc/en/Reference/Micros
[11] K. McKinney and P. Mongeau, "Multiple stage pulsed induction acceleration," *IEEE Trans. Magn.*, vol. 20, no. 2, pp. 239–242, Mar. 1984.
[12] J. Casazza and F. Delea, *Understanding Electric Power Systems: An Overview of the Technology, the Marketplace*, vol. 13. Hoboken, NJ, USA: Wiley, 2003, p. 31.

MICHAEL J. HARRIS was born in Winchester, U.K., in 1992. He received the M.Sc. degree in physics from University College London, London, U.K., in 2015.

Since 2015, he has been with the Barclays Investment Bank, London, as an Analyst.

M. SHAIKH, photograph and biography not available at the time of publication.

B. T BRISTOLL, photograph and biography not available at the time of publication.

K. VINE, photograph and biography not available at the time of publication.

PAUL A. BARTLETT was born in Portsmouth, England, in 1966. He received the B.Sc. degree (Hons.) in electronics and physics from Brighton Polytechnic, Brighton, East Sussex, U.K., in 1989, the M.Sc. degree in applied physics from the University of Hull, Kingston upon Hull, North Humberside, U.K., in 1997, and the Ph.D. degree in electronic and electrical engineering from Cardiff University, Cardiff, South Glamorgan, U.K., in 2009. This was followed by a PGDip(Ed) from University College London, London, U.K., in 2012.

He was with Wyeth Laboratories as a Chemical Analyst from 1986 to 1990, the Royal Navy as an Engineering Officer from 1993 to 1997, the Defense Evaluation and Research Agency from 1997 to 2001, and QinetiQ PLC from 2001 to 2005, and a Research Associate at Cardiff University from 2005 to 2008. He is currently a Principal Teaching Fellow with University College London, London, U.K.

Dr. Bartlett is a member of the U.K. Institute of Physics. He holds a Chartered Physicist and a Chartered Engineer designation.